Inorg. Chem. **2006**, *45*, 5703–5709

Insights into the Mechanism of Selective Olefin Epoxidation Catalyzed by $[\gamma\text{-}(SiO_4)W_{10}O_{32}H_4]^{4-}$. A Computational Study

Rajeev Prabhakar, Keiji Morokuma, Craig L. Hill, and Djamaladdin G. Musaev*

Cherry L. Emerson Center for Scientific Computation, and Department of Chemistry, Emory University, Atlanta, Georgia 30322

Received April 28, 2006

A mechanism for the H_2O_2-based epoxidation of olefins catalyzed by the lacunary polyoxometalate (POM) $[\gamma\text{-}(SiO_4)W_{10}O_{32}H_4]^{4-}$ (**1**) has been investigated at the DFT level. In this study, for the first time a "hydroperoxy" mechanism for this important process has been proposed. It is divided into two steps and investigated using the whole lacunary compound as a model. In the first step, a hydroperoxy (W–OOH) species and a water molecule are generated. The formation of this nonradical oxidant (W–OOH), consistent with the experimental suggestions, occurs with a barrier of 4.4 (7.2) kcal/mol (the number without parenthesis includes solvent effects in benzene, while the one with parenthesis is in the gas phase). In the second step, the O–O bond of the W–OOH species is cleaved, and an epoxide is formed. This step has a barrier of 38.7 (40.0) kcal/mol. It was found that the presence of one and two $(CH_3)_4N^+$ countercations significantly reduces the rate-limiting barrier by 7.6 (8.3) and 11.9 (12.6) kcal/mol, respectively, and makes this lacunary POM a very efficient catalyst for epoxidation of olefins by hydrogen peroxide. It was demonstrated that the lacunary polyoxometalate basically acts as a mononuclear W(VI) complex in activating the oxidant, a conceptually noteworthy finding.

I. Introduction

Direct epoxidation of olefins by hydrogen peroxide has been a long-standing goal of industry and synthetic organic chemistry. Epoxides are commonly used as raw material for the production of paints, epoxy resins, and surfactants.[1] Over the years, a number of environmentally hazardous epoxidation processes that utilize a variety of catalysts and oxidants have been developed, but the use of hydrogen peroxide offers an environmentally and economically attractive alternative.[2−6] The advantages of catalytic epoxidation of olefins with H_2O_2 are derived from the low cost, a high active oxygen content of this oxidant, and the production of water as the only byproduct.[7] In the search for an efficient catalyst for H_2O_2 and O_2-based epoxidations, several transition metal-containing materials, including non-heme iron complexes,[8−12] metalloporphyrins,[13] titanium silicalites,[14] methyl trioxorhenium,[15−17] tungsten compounds,[2,18,19] manganese complexes,[20] and polyoxometalates (POMs)[3−6,21−29] have been used under either homogeneous or heterogeneous conditions, but all

* To whom correspondence should be addressed. E-mail: dmusaev@emory.edu. Phone: 404-727-2382.

(1) Tullo, A. *Chem. Eng. News.* **2004**, *82*, 15.
(2) Ishii, Y.; Yamawaki, K.; Ura, T.; Yamada, H.; Yishida, T.; Ogawa, M. *J. Org. Chem.* **1988**, *53*, 3587−3593.
(3) Neumann, R.; Gara, M. *J. Am. Chem. Soc.* **1995**, *117*, 5066−5074.
(4) Mizuno, N.; Nozaki, C.; Kiyoto, I.; Misono, M. *J. Am. Chem. Soc.* **1998**, *120*, 9267−9272.
(5) Hill, C. L.; Prosser-McCartha, C. M. *Coord. Chem. Rev.* **1995**, *143*, 407−455.
(6) Kozhevnikov, I. V. *Chem. Rev.* **1998**, *98*, 171−198.
(7) Lane, B. S.; Burgess, K. *Chem. Rev.* **1989**, *89*, 2457−2760.
(8) White, M. C.; Doyle, A. G.; Jacobsen, E. N. *J. Am. Chem. Soc.* **2001**, *123*, 7194−7195.
(9) Que, L., Jr. *Science* **1991**, *253*, 273−274.
(10) Pestovsky, O.; Stoian, S.; Bominaar, E. L.; Shan, X.; Munck, E.; Que, L., Jr.; Bakac, A. *Angew. Chem., Int. Ed.* **2005**, *44*, 6871−6874.
(11) Bukowski, M. R.; Koehntop, K. D.; Stubna, A.; Bominaar, E. L.; Halfen, J. A.; Muenck, E.; Nam, W.; Que, L., Jr. *Science* **2005**, *310*, 1000−1002.
(12) MacBeth, C. E.; Golombek, A. P.; Young, V. G., Jr.; Yang, C.; Kuczera, K.; Hendrich, M. P.; Borovik, A. S. *Science* **2000**, *289*, 938−941.
(13) Battioni, P.; Renaud, J. P.; Bartoli, J. F.; Reinaartiles, M.; Fort, M.; Mansuy, D. *J. Am. Chem. Soc.* **1988**, *110*, 8462−8470.
(14) Notari, B. *Adv. Catal.* **1996**, *41*, 253.
(15) Romao, C. C.; Kühn, F. E.; Herrmann, W. A. *Chem. Rev.* **1997**, *97*, 3197−3246.
(16) Vasbinder, M. J.; Espenson, J. H. *Organometallics* **2004**, *23*, 3355−3358.
(17) Oesz, K.; Espenson, J. H. *Inorg. Chem.* **2003**, *42*, 8122−8124.
(18) Venturello, C.; Alneri, E.; Ricci, M. *J. Org. Chem.* **1983**, *48*, 3831−3833.
(19) Duncan, D. C.; Chambers, R. C.; Hecht, E.; Hill, C. L. *J. Am. Chem. Soc.* **1995**, *117*, 681−691.
(20) De Vos, D. E.; Meinershagen, J. L.; Bein, T. *Angew. Chem., Int. Ed. Engl.* **1996**, *35*, 2211−2213.
(21) Newmann, R. *Prog. Inorg. Chem.* **1998**, *47*, 317.

10.1021/ic060725p CCC: $33.50
Published on Web 06/03/2006

Table 1. Dielectric Effects of Heptane, Benzene, and Acetonitrile Solvents on All Structures

structures	gas phase	heptane ($\epsilon = 1.92$)	benzene ($\epsilon = 2.25$)	acetonitrile ($\epsilon = 36.64$)
$\mathbf{I_f}$	0.0	0.0	0.0	0.0
$\mathbf{TS_{1f}}$	7.2	4.8	4.4	3.9
$\mathbf{II_f}$	3.9	3.3	3.2	3.3
$\mathbf{TS_{2f}}$	40.0	38.3	38.7	37.9
$\mathbf{III_f}$	−32.3	−34.5	−35.2	−38.8

these systems have certain disadvantages. Recently a lacunary (a cavity-containing or "defect") Keggin-type silicodecatungstate $[\gamma\text{-}(SiO_4)W_{10}O_{32}H_4]^{4-}$ compound was reported to catalyze the epoxidation of olefins with 99% selectivity, 99% H_2O_2 utilization efficiency, and high stereospecificity. Furthermore, the catalyst is easily recovered at 305 K.[26,30] This epoxidation process using C_2H_4 as a substrate can be described by eq 1. Significantly however, very little is known,

$$C_2H_4 + H_2O_2 \rightarrow C_2H_4O + H_2O \qquad (1)$$

both experimentally and theoretically, about the mechanism of this promising POM-catalyzed H_2O_2-based epoxidation chemistry. All the experimentally available information concerning this chemistry can be summarized as follows: (1) There are four Me_4N^+ countercations per lacunary compound. One should note that, in the paper by Mizuno et al. (ref 30), the structural analysis of $[\gamma\text{-}(SiO_4)W_{10}O_{32}H_4]^{4-}$ was of the tetramethylammonium, $(Me_4N)_4$, salt, while all the epoxidation data provided in Table 1 and discussed in the paper were obtained using the $(Bu_4N)_4$ salt. (2) The high stereospecificity of the alkene oxidation suggests a structurally rigid and nonradical substrate-attacking intermediate, and (3) diepoxide is not produced in diene oxidations.[30]

Unfortunately, the aforementioned experimental information sheds little light on the catalytic mechanism of this reaction. These experiments in aggregate do not elaborate the nature and structures of intermediates and transitions states or the effect of countercations on the rate of the reaction. Ion pairing is largely ignored in studies of the POM-catalyzed epoxidation process, but it could impact both rate and selectivity.[27,31,32] Therefore, in this paper we investigate the mechanism of the $[\gamma\text{-}(SiO_4)W_{10}O_{32}H_4]^{4-}$-catalyzed epoxidation of olefins by H_2O_2 at the DFT level. A recent B3LYP study of this compound indicated that it possessed four terminal hydroxyl ligands, $[\gamma\text{-}(SiO_4)W_{10}O_{28}(OH)_4]^{4-}$ (**1**), rather than the previously suggested two aqua and two oxo (terminal) ligands (i.e., $[\gamma\text{-}(SiO_4)W_{10}O_{28}(H_2O)_2]^{4-}$).[33] The reported asymmetry in the W−O (terminal) bond distances of $[\gamma\text{-}(SiO_4)W_{10}O_{32}H_4]^{4-}$ was explained in terms of the existence of $O^1H^{1\cdots}O^2H^2$ and $O^4H^{4\cdots}O^3H^3$ hydrogen-bonding patterns in the $[\gamma\text{-}(SiO_4)W_{10}O_{28}(OH)_4]^{4-}$ structure. In the present study, the mechanism of olefin epoxidation by hydrogen peroxide catalyzed by **1** is addressed in detail for the first time.

II. Computational Details

A. Methods. All calculations were performed using the Gaussian 03 program.[34] The geometries of the reactants, intermediates, transition states, and products were optimized without any symmetry constraints at the B3LYP/Lanl2dz level of theory with additional d polarization functions for the Si atom ($\alpha = 0.55$) and the corresponding Hay−Wadt effective core potential (ECP) for W.[35,36] The final energetics of the optimized structures were further improved by performing single-point calculations including additional d and p polarization functions for the O ($\alpha = 0.96$) and H ($\alpha = 0.36$) atoms, respectively, in the basis set used for optimizations.

The dielectric effects from the surrounding environment were estimated using the self-consistent reaction field IEF−PCM method[37] at the B3LYP/Lanl2dz level with d polarization functions for the Si atom. Since the catalyst was prepared at pH 2,[30] we used a variety of solvents with dielectric constants of 1.92, 2.25, and 36.64 corresponding to heptane, benzene, and acetonitrile, respectively. The dielectric effects of all these solvents are shown in Table 1, and it was found that they all exhibit very similar effects (i.e., 0.1−0.4 kcal/mol on transition states and 0.1−4.3 kcal/mol on minima). Throughout the paper, we use the B3LYP/{Lanl2dz + d(Si,O) + p(H)} energies including the zero-point vibrational (unscaled), thermal (at 298.15 K and 1 atm), entropy corrections (at 298.15 K), and solvent effects in benzene, while the energies without solvent effects are provided in parentheses.

B. Models. Compound **1** is a large molecule bearing four hydroxyl (−OH) groups, which are expected to participate in the

(22) (a) Neumann, R.; Dahan, M. *Nature* **1997**, *388*, 353−355. (b) Neumann, R.; Dahan, M. *J. Am. Chem. Soc.* **1998**, *120*, 11969−11976.
(23) Nishiyama, Y.; Nakagawa, Y.; Mizuno, N. *Angew. Chem., Int. Ed.* **2001**, *19*, 3751−3753.
(24) Okun, N. M.; Anderson, T. M.; Hill, C. L. *J. Am. Chem. Soc.* **2003**, *125*, 3194−3195.
(25) Weinstock, I. A.; Barbuzzi, E. M. G.; Wemple, M. W.; Cowan, J. J.; Reiner, R. S.; Sonnen, D. M.; Heintz, R. A.; Bond, J. S.; Hill, C. L. *Nature* **2001**, *414*, 191−195.
(26) Nakagawa, Y.; Kamata, K.; Kotani, M.; Yamaguchi, K.; Mizuno, N. *Angew. Chem., Int. Ed.* **2005**, *44*, 5136−5141.
(27) Hill, C. L. In *Comprehensive Coordination Chemistry II*; Wedd, A. G., Ed.; Elsevier Science: New York, 2004; Vol. 4, pp 679−759.
(28) Neumann, R. *Prog. Inorg. Chem.* **1998**, *47*, 317−370.
(29) Neumann, R. In *Modern Oxidation Methods*; Bäckvall, J.-E., Ed.; John Wiley & Sons: New York, 2004.
(30) Kamata, K.; Yonehara, K.; Sumida, Y.; Yamahuchi, K.; Hikichi, S.; Mizuno, N. *Science* **2003**, *300*, 964−966.
(31) Grigoriev, V. A.; Cheng, D.; Hill, C. L.; Weinstock, I. A. *J. Am. Chem. Soc.* **2001**, *123*, 5292−5307.
(32) Kirby, J. F.; Baker, L. C. W. *Inorg. Chem.* **1998**, *37*, 5537−5543.
(33) Musaev, D. G.; Morokuma, K.; Geletii, Y. V.; Hill, C. L. *Inorg. Chem.* **2004**, *43*, 7702−7708.
(34) Frisch, M. J.; Trucks, G. W.; Schlegel, H. B.; Scuseria, G. E.; Robb, M. A.; Cheeseman, J. R.; Montgomery, J. A., Jr.; Vreven, T.; Kudin, K. N.; Burant, J. C.; Millam, J. M.; Iyengar, S. S.; Tomasi, J.; Barone, V.; Mennucci, B.; Cossi, M.; Scalmani, G.; Rega, N.; Petersson, G. A.; Nakatsuji, H.; Hada, M.; Ehara, M.; Toyota, K.; Fukuda, R.; Hasegawa, J.; Ishida, M.; Nakajima, T.; Honda, Y.; Kitao, O.; Nakai, H.; Klene, M.; Li, X.; Knox, J. E.; Hratchian, H. P.; Cross, J. B.; Bakken, V.; Adamo, C.; Jaramillo, J.; Gomperts, R.; Stratmann, R. E.; Yazyev, O.; Austin, A. J.; Cammi, R.; Pomelli, C.; Ochterski, J. W.; Ayala, P. Y.; Morokuma, K.; Voth, G. A.; Salvador, P.; Dannenberg, J. J.; Zakrzewski, V. G.; Dapprich, S.; Daniels, A. D.; Strain, M. C.; Farkas, O.; Malick, D. K.; Rabuck, A. D.; Raghavachari, K.; Foresman, J. B.; Ortiz, J. V.; Cui, Q.; Baboul, A. G.; Clifford, S.; Cioslowski, J.; Stefanov, B. B.; Liu, G.; Liashenko, A.; Piskorz, P.; Komaromi, I.; Martin, R. L.; Fox, D. J.; Keith, T.; Al-Laham, M. A.; Peng, C. Y.; Nanayakkara, A.; Challacombe, M.; Gill, P. M. W.; Johnson, B.; Chen, W.; Wong, M. W.; Gonzalez, C.; Pople, J. A. *Gaussian 03*, revision C1; Gaussian, Inc.: Wallingford, CT, 2004.
(35) (a) Becke, A. D. *Phys. Rev. A* **1988**, *38*, 3098−3107. (b) Lee, C.; Yang, W.; Parr, R. G. *Phys. Rev. B* **1988**, *37*, 785−789. (c) Becke, A. D. *J. Chem. Phys.* **1993**, *98*, 5648.
(36) Hay, P. J.; Wadt, W. R. *J. Chem. Phys.* **1985**, *82*, 270−283.
(37) Cances, E.; Mennucci, B.; Tomasi, J. *J. Chem. Phys.* **1997**, *107*, 3032−3041.

Scheme 1. Small and Full Models of the Lacunary $[\gamma\text{-}(SiO_4)W_{10}O_{28}(OH)_4]^{4-}$ Polyoxometalate

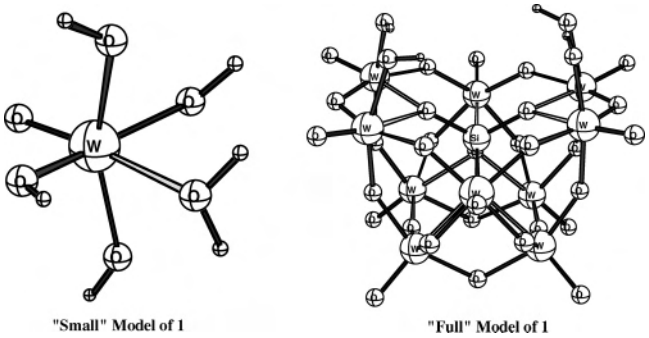

catalysis. Therefore, in this study, two different models ("small" and "full") of **1** are used (see Scheme 1).

Our small model incorporates only one such site including only one W atom coordinated to an oxo group (═O), four hydroxyl groups (−OH), and a water molecule (aqua ligand). In this model, the three hydroxyl groups are added to keep the overall charge on the system neutral; the water molecule represents the remaining part of the lacunary compound. It should be noted that this is a very simple model of structurally complicated **1** and could provide unreliable results. Nonetheless, this model allows us to probe the possible mechanisms for H_2O_2-based olefin epoxidation catalyzed by **1**. The results obtained from this small model are then evaluated using a full model, which includes the entire structure of **1**. In these calculations, C_2H_4 is used to model olefins, and up to two explicit Me_4N^+ molecules have been used to calculate the countercation effects. The overall charge of the system is 4−, and as shown previously, it exists in a singlet ground electronic state.[33]

III. Results and Discussion

The computed exothermicity of reaction 1 is 38.2 (37.5) kcal/mol. Since there is no information concerning the mechanism of the epoxidation catalyzed by $[\gamma\text{-}(SiO_4)W_{10}O_{28}(OH)_4]$,$^{4-}$ we initially used, as noted above, the small model to identify the possible mechanisms. In our preliminary investigations, as discussed below, the formation of peroxo, superoxo, and hydroperoxo species was considered. For the generation of the peroxo species, H_2O_2 has to donate both its protons, and there are no obvious proton acceptors in the neighborhood of **1**. Moreover, a peroxo species is highly reactive and will start abstracting protons from the hydroxyl groups bonded to the W atoms and alter their oxidation states. This situation would contradict the experimental proposal that a structurally rigid intermediate is generated during the reaction.[30] On the other hand, the generation of a superoxide will require the formation of a radical pair which is clearly ruled out by experiments suggesting the creation of a nonradical substrate-attacking intermediate.[30] Furthermore, the barrier for the cleavage of the W═O bond to form epoxide was calculated to be prohibitively high. Finally, after preliminary investigations, a "hydroperoxy" mechanism incorporating all the available experimental and theoretical information was chosen for further studies. Recently, NMR data for polyoxovanadometalate $[\gamma\text{-}1,2\text{-}H_2SiV_2W_{10}O_{40}]^{4-}$-catalyzed epoxidation of olefins by hydrogen peroxide also indicated the formation of a {VO-(μ-OH)(μ-OOH)-VO} type of hydroperoxy species.[38] This mechanism incorporates the following two steps: (1) formation of a W−hydroperoxy (W−OOH) species and (2) formation of epoxide.

A. Small Model Investigations. Formation of W−Hydroperoxy (W−OOH) Species. At the starting point of this step, H_2O_2 and C_2H_4 bind to the lacunary compound to form complex $\mathbf{I_s}$ (where the subscript s denotes the small model, Figure 1).

In this structure ($\mathbf{I_s}$), H_2O_2 forms strong hydrogen bonds with the distal hydroxyl ($-O^1H$) and the aqua ligand with bond distances of $O^1H = 1.41$ Å and $O^3H = 1.68$ Å, respectively. Simultaneously, C_2H_4 weakly interacts with the hydrogen atom of the same distal hydroxyl group ($-O^1H$). At this point, in a concerted manner, the O^2-H bond of H_2O_2 is broken, and the proton is transferred to the distal hydroxyl group ($-O^1H$). This process leads to the formation of a hydroperoxide ($-O^2O^3H$) and a water molecule. The resulting $-O^2O^3H$ in turn makes a nucleophilic attack at the vacant site (created as the result of water formation and dissociation) on the metal center to generate a W−hydroperoxy (W−O^2O^3H) species ($\mathbf{II_s}$). The optimized transition state ($\mathbf{TS1_s}$) for this process is shown in Figure 1, and this step has a barrier of 10.5 (11.1) kcal/mol. In $\mathbf{TS1_s}$, all the corresponding distances ($O^2H = 1.50$ Å, $O^1H = 1.06$ Å, and $W-O^1H = 2.25$ Å) indicate proton migration from H_2O_2 to O^1H and the formation of a water molecule. The connections between $\mathbf{TS1_s}$ and the corresponding minima are confirmed by the intrinsic reaction coordinate (IRC)[39] calculations. The formation of the W-bound hydroperoxy species is slightly exothermic by 0.2 (0.4) kcal/mol.

Formation of Epoxide. In this step of the hydroperoxy mechanism, the intermediate W−O^2O^3H species reacts with C_2H_4 to produce ethylene epoxide ($C_2H_4O^3$). Here, in a concerted fashion, the O^3-H bond of the W−O^2O^3H species is broken, and the proton is transferred through a water molecule to the W-bound oxygen atom (W−O^2). In this process, the O^2-O^3 bond of the W−O^2O^3H species is cleaved, and the released oxygen atom (O^3) is immediately abstracted by the C_2H_4 molecule to form an epoxide. The optimized transition state structure ($\mathbf{TS2_s}$) is shown in Figure 1, and this process has a barrier of 26.9 (32.0) kcal/mol. All the corresponding bond distances ($O^3H = 1.05$ Å, $O^1H = 1.49$ Å, $O^2-O^3 = 1.96$ Å, and $C-O^3 = 1.83$ Å) indicate that this is a synchronous process. This step has some similarities to the O−O bond splitting of the Fe(II)−(HOOH) species in the peroxidase pathway of cytochrome P450. In this enzyme, the distal His has been suggested to play the role of an intermediate catalyst by accepting a proton from the proximal oxygen and then donating it to the distal oxygen.[40] In the present study, a water molecule has been proposed to perform a role similar to that of the distal His in cytochrome P450, as a proton donor and acceptor. Another example of such a process is the O−O bond cleavage of the

(38) Nakagawa, Y.; Kamata, K.; Kotani, M.; Yamaguchi, K.; Mizuno, N. *Angew. Chem., Int. Ed.* **2005**, *44*, 5136−5141.
(39) Gonzalez, C.; Schlegel, H. B. *J. Phys. Chem.* **1990**, *94*, 7467−7471.
(40) Denisov, I. G.; Makris, T. M.; Sligar, S. G.; Schlichting, I. *Chem. Rev.* **2005**, *105*, 2253−2278.

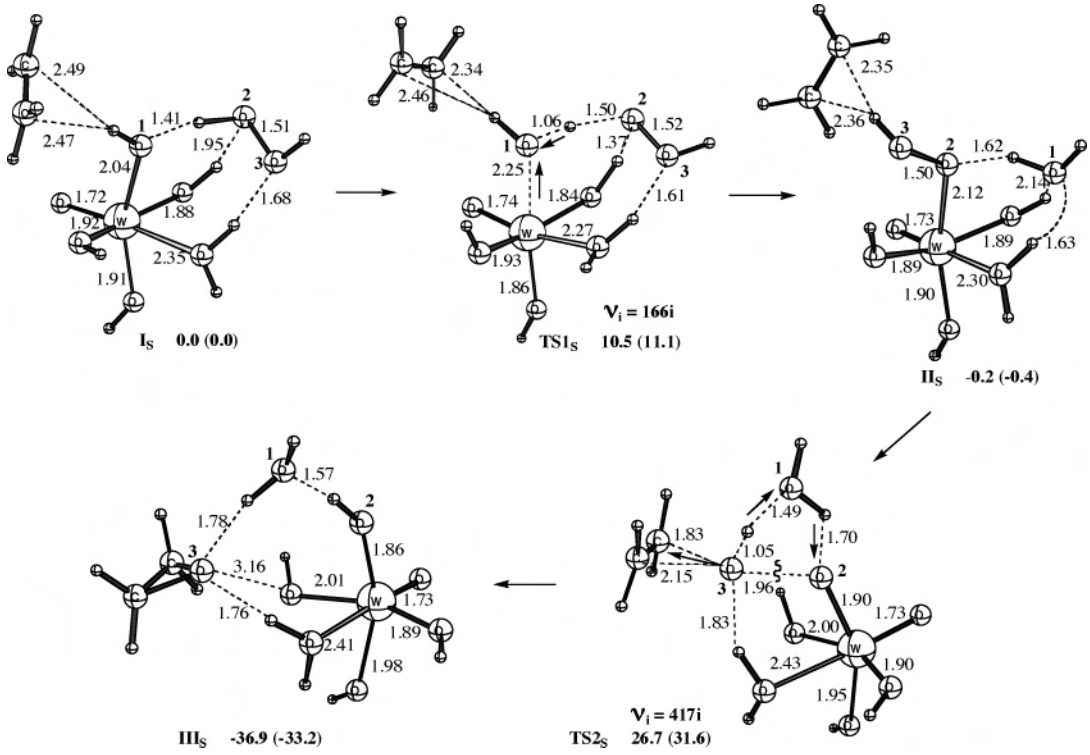

Figure 1. Optimized structures (in Å) and energies [with and without (in parentheses) solvent effects in kcal/mol] of the reactant, intermediates, transition states, and the product for the small model of the $[\gamma\text{-}(SiO_4)W_{10}O_{28}(OH)_4]^{4-}$ polyoxometalate.

Cu(II)−OOH species in copper amine oxidase (CAO).[41] In CAO, indirectly through a water molecule, a proton transfer from a sp^3 carbon of the phenol ring to one of the oxygens of the peroxide splits the O−O bond and creates a Cu(II)−OH species. The transition structure (**TS2$_s$**) is also confirmed to be connected to the corresponding minima by IRC calculations. The formation of the epoxide product (structure **III$_s$**, Figure 1) in this process is calculated to be exothermic by 36.7 (32.8) kcal/mol relative to the **II$_s$** reactant.

Although the barrier for this mechanism is high 26.9 (32.0) kcal/mol, it is a certainly worthwhile to examine this mechanism using the more realistic full model. To include the effects of the whole lacunary polyoxometalate structure and four Me_4N^+ countercations in the calculations, this mechanism has been investigated using the full model of **1** and up to two molecules of the Me_4N^+ cation.

B. Full Model Investigations. It is noteworthy that, in this study, we use the tetrahydroxyl, $[\gamma\text{-}(SiO_4)W_{10}O_{28}(OH)_4]^{4-}$, form of **1**, $[\gamma\text{-}(SiO_4)W_{10}O_{32}H_4]$,[4] rather than the experimentally reported[30] bis(oxo) and bis(aquo), $[\gamma\text{-}(SiO_4)W_{10}O_{28}(H_2O)_2]$,$^{4-}$ form. The choice of this model is based on our previous computational study[33] which clearly demonstrated, by incorporating the available experimental data, that the $[\gamma\text{-}(SiO_4)W_{10}O_{28}(OH)_4]^{4-}$ form of **1** is energetically more favorable than the $[\gamma\text{-}(SiO_4)W_{10}O_{28}(H_2O)_2]^{4-}$ form. Thus, our full model has the four hydroxyl (−OH) groups representing the possible reaction sites, but we have used only one such site to probe the mechanism. As demonstrated in the case of the small model studies, the first step of the investigated hydroperoxy mechanism is the formation of the W−hydroperoxy species.

Formation of the W−hydroperoxy (W−OOH) Species. In this step of the reaction, H_2O_2 and C_2H_4 are bonded to the lacunary compound to form complex **I$_f$** (where subscript f denotes the full model, Figure 2).

The mode of H_2O_2 binding in **I$_f$** is slightly different than that in **I$_s$**. In **I$_f$**, H_2O_2 forms strong hydrogen bonds with a hydroxyl ($-O^1H$) group and a terminal oxo (W═O) group of the lacunary compound, whereas C_2H_4 binds in exactly the same manner with the hydroxyl group. However, similar to that for the small model, the O^2-H bond of H_2O_2 is broken, and the hydroperoxide ($W-O^2O^3H$) species and a water molecule are generated (structure **II$_f$**, Figure 2). The optimized transition state (**TS1$_f$**) for this process is shown in Figure 2, and this step has a barrier of 4.4 (7.2) kcal/mol. Thus, the inclusion of the full lacunary complex reduces the barrier by 6.1 kcal/mol. In **TS1$_f$**, the O^2-H bond is activated (O^2-H bond distance = 1.04 Å), and the corresponding $W-O^1H$ distance of 2.00 Å, which is slightly longer than the other W−OH (1.95 Å) bond distances, indicates the formation of a water molecule. All critical distances in **TS1$_f$** are very similar to those in **TS1$_s$**, which have been confirmed to be connected with both the reactant and the product (**I$_s$** and **II$_s$**) by IRC calculations. The formation of the $W-O^2O^3H$ species is a slightly endothermic by 3.2 (3.9) kcal/mol. The formation of this species is in line with the experimental suggestions that a nonradical oxidant is generated on the lacunary compound, and only a water molecule is produced as the byproduct.[30] It should be noted that the formation of the $W-O^2O^3H$ species is possible only if an −OH group is

(41) Prabhakar, R.; Siegbahn, P. E. M. *J. Am. Chem. Soc.* **2004**, *126*, 3996−4006.

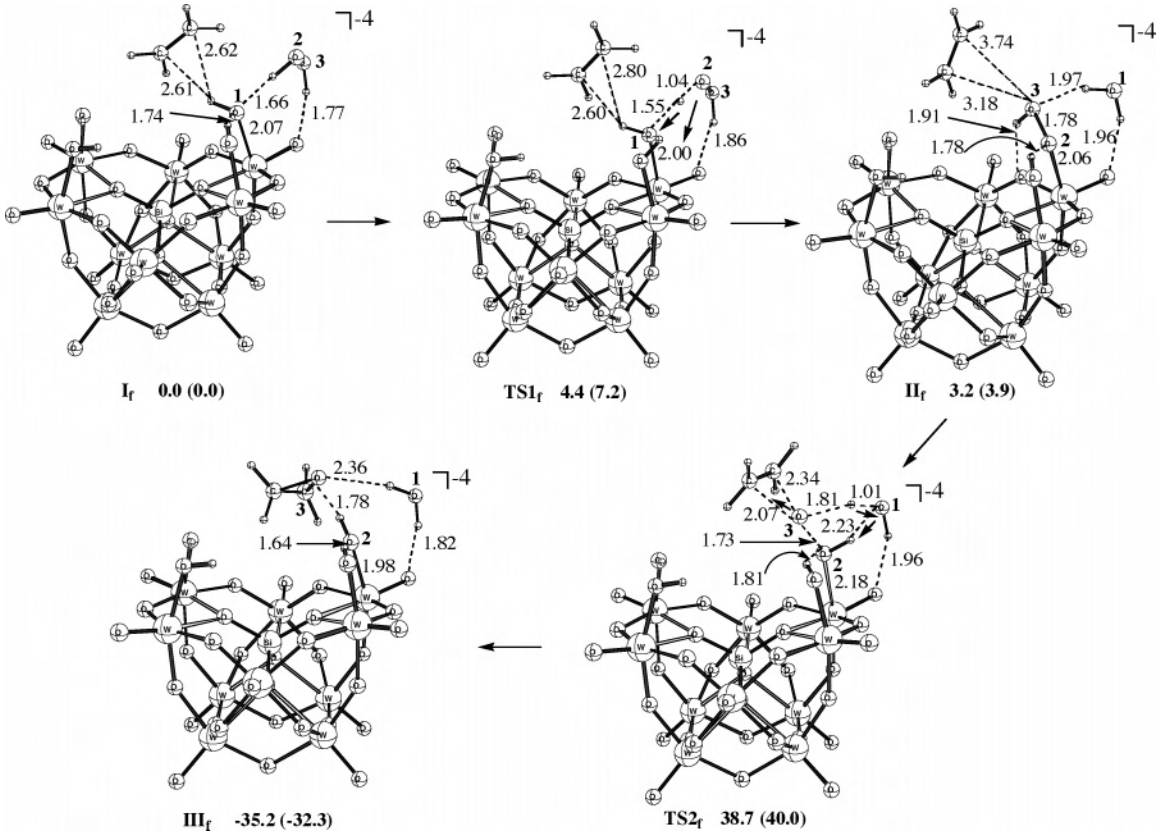

Figure 2. Optimized structures (in Å) and energies [with and without (in parentheses) solvent effects in kcal/mol] of the reactant, intermediates, transition states, and the product for the full model of the $[\gamma\text{-}(SiO_4)W_{10}O_{28}(OH)_4]^{4-}$ polyoxometalate.

coordinated to the W. This also supports the conclusion of our previous study that instead of two aqua and two oxo (terminal) groups, **1** prefers to have four terminal hydroxo ligands.[33]

Formation of the Epoxide. After $W-O^2O^3H$ formation, the ethylene epoxide ($C_2H_4O^3$) is produced. This is the most critical step of the proposed mechanism. Here, again in the same way as in the small model, the $-O^3H$ bond of the $W-O^2O^3H$ species is broken, and the proton transfer via a water molecule to the W-bound oxygen atom ($W-O^2$) cleaves the O^2-O^3 bond and forms an epoxide. The optimized transition state structure (**$TS2_f$**) is shown in Figure 2, and the corresponding distances ($O^2-O^3 = 1.73$ Å and $C-O^3 = 2.07$ Å) indicate that this process is synchronous. The critical distances in this structure are also similar to those of **$TS2_s$** and are confirmed by IRC calculations to be connected to both the reactant and the product. The formation of the epoxide has a very high barrier of 35.5 (36.1) kcal/mol, which indicates a very low reactivity for **1**. Inclusion of the full model of the lacunary complex increases the barrier by 8.6 (4.1) kcal/mol. Moreover, this process follows a 3.2 (3.9) kcal/mol endothermic step which makes the overall barrier for this process from **I_f** 38.7 (40.0) kcal/mol. This is the rate-limiting step of the entire catalytic cycle. In the product (**III_f**), the epoxide is hydrogen bonded to the lacunary complex and the water molecule. The formation of the ethylene epoxide product from **II_f** is found to be exothermic by 38.3 (35.3) kcal/mol.

Countercation Effect. Since it has been known experimentally that four Me_4N^+ countercations per unit of **1** are present during the catalysis, their effect on the barrier of the rate-limiting process (**$I_f \rightarrow TS2_f$**) was also investigated. The countercation effects have been computed by explicitly including up to two Me_4N^+ molecules in the models. The reactant in the presence of one and two Me_4N^+ molecules (structures **I_{1CC}** and **I_{2CC}**, Figure 3) is fully optimized, whereas in the transition state structures (**$TS2_{1CC}$** and **$TS2_{2CC}$**, Figure 3), only the main reaction coordinates (O^2O^3, O^1H, O^2H, O^3H, and O^3C bond distances) from the **$TS2_f$** are kept frozen.

This type of approximation can be justified by considering the fact that the entire $[\gamma\text{-}(SiO_4)W_{10}O_{28}(OH)_4]^{4-}$ compound is already included in the calculations. Solvent effects are included in the calculated energetics by performing single-point calculations at the IEF−PCM level. The addition of the first molecule of Me_4N^+, located inside the cavity, reduces the barrier from **I_f** by 7.6 (8.3) kcal/mol, and the overall barrier for the formation of epoxide becomes 31.1 (31.7) kcal/mol. Furthermore, the inclusion of the second Me_4N^+ molecule, positioned outside the cavity, further reduces the barrier from **I_f** by 4.3 (4.3) kcal/mol, and the overall barrier becomes 26.8 (27.5) kcal/mol. The reason for the relatively small effect of the second countercation is that, in comparison to 7 hydrogen bonds formed by the first Me_4N^+ molecule, it forms only 5 hydrogen bonds with the lacunary complex. The remaining two countercations may have smaller effects, but their presence is also expected to

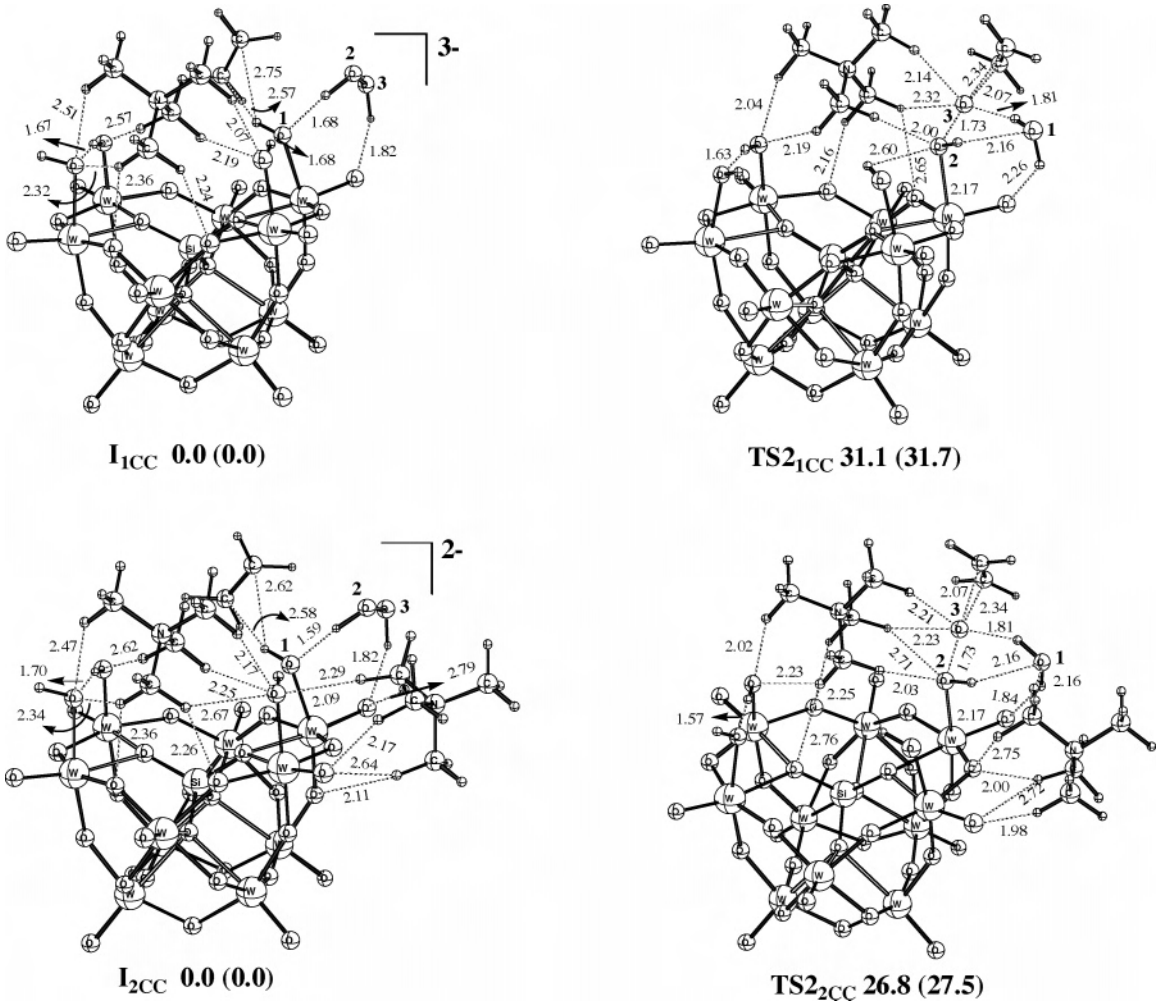

Figure 3. Optimized structures (in Å) and energies (in kcal/mol) of the reactant and the transition state in the presence of the NH_4^+ countercation for the full model of the $[\gamma\text{-}(SiO_4)W_{10}O_{28}(OH)_4]^{4-}$ polyoxometalate.

reduce the rate-limiting barrier. On the other hand, it was found that the use of the NH_4^+ ion, as a model for Me_4N^+, overestimates the countercation effects by 11.7 (10.7) kcal/mol. This pronounced countercation effect on **TS2$_f$** derives, in good measure, from the fact that the −OOH fragment of the W−OOH bears a significant negative charge which is strongly stabilized by the countercation. These results clearly indicate that the presence of countercations strongly influences the reactivity of **1** and makes it a very efficient catalyst under moderate conditions. They also suggest that ion-pairing effects in the H_2O_2-based oxidation catalyzed by POMs could be of general importance.

IV. Summary and Conclusions

In the present study, the H_2O_2-based epoxidation of C_2H_4 catalyzed by **1** has been investigated at the DFT level. Initially, the use of the small model of the lacunary POM implicates the hydroperoxy mechanism; this mechanism is then investigated with the full model of **1**. The comparison of the data for the small and full model studies indicates that the lacunary POM **1** basically acts as a mononuclear W(VI) complex in activating the oxidant.

The proposed mechanism is divided into two steps, and the energy diagram is presented in Figure 4. In the first step,

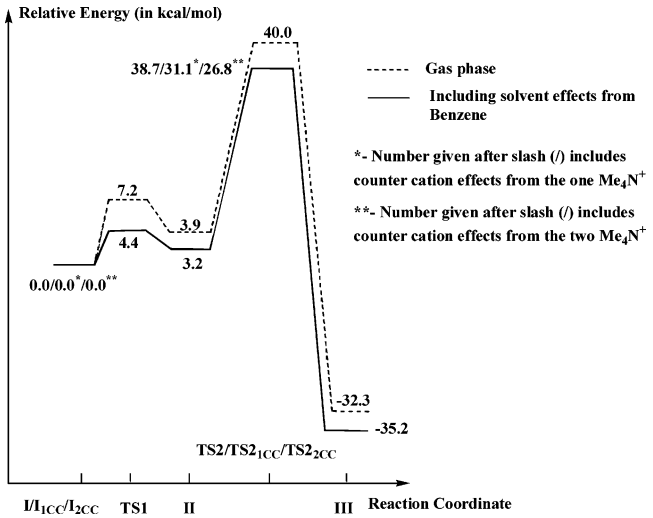

Figure 4. Energy diagram of the H_2O_2-based olefin epoxidation catalyzed by the lacunary $[\gamma\text{-}(SiO_4)W_{10}O_{28}(OH)_4]^{4-}$ polyoxometalate.

the O^2−H bond of H_2O_2 is broken, and the hydroperoxide (W−O^2O^3H) species and a water molecule are produced in a concerted manner. This process has a barrier of 4.4 (7.2) kcal/mol, and it is slightly endothermic by 3.2 (3.9) kcal/mol. The formation of the products (W−O^2O^3H and H_2O)

in this step is in agreement with experimental suggestions that a nonradical oxidant is generated on the lacunary POM and that only a water molecule is produced as a byproduct.[30]

In the second and the final step, the O^3H bond of the $W-O^2O^3H$ species is cleaved, and the proton is transferred via a water molecule to the W-bound oxygen atom ($W-O^2$) to split the O^2-O^3 bond and form an epoxide. This is the rate-limiting step of the entire catalytic cycle and occurs with an overall barrier of 38.7 (40.0) kcal/mol. The formation of the product ($C_2H_4O^3$) is exothermic by 38.3 (35.3) kcal/mol.

Since the barrier for the rate-limiting process is quite high, the effect of Me_4N^+ on the epoxidation step was examined. Compound **1** has been documented experimentally to contain four Me_4N^+ countercations. It was found that the inclusion of the one and two molecules of countercation (Me_4N^+) reduces the rate-limiting barrier by 7.6 (8.3) and 11.9 (12.6) kcal/mol, respectively. These results clearly indicate that ion-pairing interactions make **1** a more efficient catalyst for the epoxidation of C_2H_4 by H_2O_2.

This study, for the first time, provides a detailed mechanism and assesses the impact of a countercation on a POM-catalyzed H_2O_2-based epoxidation reaction. However, it needs to be mentioned that the aforementioned conclusions are based on the full model studies, where **1** was modeled as a species containing four hydroxyl (−OH) groups, rather than the bis(oxo) and bis(aquo) groups, which were previously[33] demonstrated to be energetically less favorable.

Acknowledgment. The present research is in part supported by a grant (DE-FG02-03ER15461) from the Department of Energy. Acknowledgment is made to the Cherry L. Emerson Center of Emory University for the use of its resources.

Supporting Information Available: Tables S1−S5 showing the Cartesian coordinates (in Å) of all the optimized structures including the transition states using the small model, Tables S5−S10 showing the Cartesian coordinates (in Å) of all the optimized structures including the transition states using the full model, Tables S11−S14 showing the Cartesian coordinates (in Å) of the optimized reactant ($\mathbf{I_f}$) and transition state ($\mathbf{TS2_f}$) including 1 and 2 molecules of Me_4N^+ countercation, Tables S15 and S16 shwoing the Cartesian coordinates (in Å) of the optimized reactant ($\mathbf{I_f}$) and transition state ($\mathbf{TS2_f}$) including the NH_4^+ countercation, and Figures S1 and S2 showing the structures of the optimized reactant ($\mathbf{I_f}$) and transition state ($\mathbf{TS2_f}$) and a potential energy surface for NH_4^+. This material is available free of charge via the Internet at http://pubs.acs.org.

IC060725P